Letter

Magnetism and electronic structure of a Dy adatom on a MgO(001) substrate

Alexander B. Shick,[1,2] Eduard Belsch,[1,3] and Alexander I. Lichtenstein[3,4]
[1]*Institute of Physics, Czech Academy of Sciences, Na Slovance 2, 182 21 Prague, Czech Republic*
[2]*Department of Molecular Chemistry and Materials Science, Weizmann Institute of Science, Rehovoth 76100, Israel*
[3]*Institute of Theoretical Physics, University of Hamburg, 20355 Hamburg, Germany*
[4]*European X-Ray Free-Electron Laser Facility, Holzkoppel 4, 22869 Schenefeld, Germany*

(Received 26 June 2023; revised 22 September 2023; accepted 6 November 2023; published 27 November 2023)

The electronic structure and magnetism of an individual Dy atom adsorbed on the MgO(001) substrate is investigated using a combination of the density functional theory with the Hubbard-I approximation to the Anderson impurity model. The divalent Dy^{2+} adatom in f^{10} configuration is found. The calculated x-ray absorption and magnetic circular dichroism spectra are compared to the experimental data. Quantum tunneling between degenerate $|J = 8.0, J_z = \pm 4.0\rangle$ states leads to the formation of a $|J = 8.0, J_z = 0.0\rangle$ ground state with an in-plane orientation of the magnetic moment. It explains the absence of remanent magnetization in a Dy adatom on the top of the MgO(001) substrate. Our studies can provide a viable route for further investigation and prediction of the rare-earth single-atom magnets.

DOI: 10.1103/PhysRevB.108.L180408

Lanthanide atom adsorption on suitable surfaces is a viable pathway for creating atomic scale magnetic memories [1] and quantum logic devices [2]. Dysprosium (Dy) exhibits a large magnetic anisotropy and can be protected against quantum tunneling in a uniaxial crystal field [3]. It has been used for molecular magnets with record-high blocking temperature [4], and the surface adsorbed single-atom magnets with a long magnetization lifetime [5].

Recently, it was shown experimentally [6] that the electronic properties of Dy adatoms on MgO thin films grown on the top of metal Ag(001) substrate change with the thickness of the supporting MgO layer. X-ray absorption spectroscopy (XAS) and magnetic circular dichroism (XMCD) at 2.5 K reveal a predominance of bulklike $4f^9$ Dy for Dy@MgO/Ag(001) with the MgO layer thickness less than 5 ML. By an increase of the MgO layer thickness, Dy atoms acquire the $4f^{10}$ configuration. They display the butterfly-type magnetic hysteresis loop, indicating quantum tunneling of the magnetization (QTM).

Despite the relatively simple coordination of the atom support structure, it remains challenging to predict theoretically an influence of the substrate and adsorption geometry on the Dy $4f$-shell charge and magnetic configurations. Theoretical calculations often require prior knowledge of the experimental data [6]. Density functional theory (DFT) is used to obtain the optimized adsorption geometry. The XAS spectra are then fitted making use of MultiX multiplet calculations [7] together with a point charge model with the positions and values of the Born charges deduced from DFT.

In this work, we present an alternative theoretical approach, based on the combination of relativistic DFT with the multiorbital impurity Hamiltonian, and we apply it to investigate the electronic and magnetic character of a Dy adatom at MgO(001). Our calculations suggest that the multiconfigurational aspect of the Dy $4f$-shell together with a correct atomic limit need to be taken into account in order to reproduce the magnetic and spectroscopic properties of Dy@MgO.

The DFT+U correlated electronic structure theory in a rotationally invariant, full potential implementation [8,9] minimizes the total energy functional

$$E^{\mathrm{tot}}(\rho, \hat{n}) = E^{\mathrm{DFT}}(\rho) + E^{\mathrm{ee}}(\hat{n}) - E^{\mathrm{dc}}(\hat{n}), \tag{1}$$

where $E^{\mathrm{DFT}}(\rho)$ is the usual density functional of the total electron and spin densities, $\rho(\mathbf{r})$, including SOC. E^{ee} is an electron-electron interaction energy, and E^{dc} is a "double-counting" term, which accounts approximately for an electron-electron interaction energy already included in E^{DFT}. Both are functions of the local orbital occupation matrix $\hat{n} = n_{\gamma_1\gamma_2}$ in the subspace of the f spin-orbitals $\{\phi_\gamma = \phi_{m\sigma}\}$.

Minimization of the DFT+U total energy functional Eq. (1) leads to the solution of the generalized Kohn-Sham-Dirac equations,

$$[-\nabla^2 + V_{\mathrm{DFT}}(\mathbf{r}) + (V_U - V_{\mathrm{dc}}) + \xi(\mathbf{l}\cdot\mathbf{s})]\Phi_{\mathbf{k}}(\mathbf{r}) = \epsilon_{\mathbf{k}}\Phi_{\mathbf{k}}(\mathbf{r}), \tag{2}$$

where V_U is an effective DFT+U potential, and V_{dc} is the spherically symmetric DFT+U double-counting term [10,11] The self-consistent solution of Eq. (2) generates not only the ground-state energy and charge/spin densities, but also effective one-electron states and energies. The basic difference of DFT+U calculations from DFT is their explicit dependence on the on-site spin- and orbitally resolved $n_{\gamma_1\gamma_2}$ occupation matrices.

The fundamental limitation of DFT+U calculations is that they rely on a single Slater determinant approximation for the f-manifold. However, as pointed out in Refs. [13,14], it makes the DFT+U results extremely sensitive to the initial conditions, which leads to numerous metastable solutions.

To avoid convergence to a metastable state, various strategies have been proposed. The occupation matrix control (OMC) has recently been exploited by Krack [15] for the

two f-electrons, however the identified ground state does not agree with earlier DFT+U results of Dorado *et al.* [16]. Alternatively, the so-called U-ramping method relies on a gradual increase of the Coulomb-U parameter of DFT+U. While this approach has had some success, it has been shown to give higher energies than the OMC method [17].

Recently, we proposed the extension of DFT+U [18] making use of a combination of DFT with the exact diagonalization of the Anderson impurity model [19]. The complete seven-orbital $4f$ shell model includes the full spherically symmetric Coulomb interaction, the spin-orbit coupling, and the crystal field. The corresponding Hamiltonian can be written as

$$\hat{H}_{\rm imp} = \sum_{m\sigma} \epsilon_f f^\dagger_{m\sigma} f_{m\sigma} + \sum_{mm'\sigma\sigma'} \left[\xi \mathbf{l}\cdot\mathbf{s} + \hat{\Delta}_{\rm CF} + \frac{\Delta_{\rm EX}}{2}\hat{\sigma}_z \right]^{\sigma\ \sigma'}_{mm'} f^\dagger_{m\sigma} f_{m'\sigma'} + \frac{1}{2}\sum_{\substack{mm'm''\\ m'''\sigma\sigma'}} U_{mm'm''m'''} f^\dagger_{m\sigma} f^\dagger_{m'\sigma'} f_{m'''\sigma'} f_{m''\sigma}, \quad (3)$$

where $f^\dagger_{m\sigma}$ creates a $4f$ electron. The ξ parameter specifies the SOC strength, and it is taken from DFT calculations in a standard way [20], making use of the radial solutions of the Kohn-Sham-Dirac scalar-relativistic equations (2), and the radial derivative of the spherically symmetric part of the DFT potential. $\Delta_{\rm CF}$ is the crystal-field potential, and $\Delta_{\rm EX}$ is the exchange field strength. The parameter ϵ_f ($= -\mu$, the chemical potential) defines the number of f-electrons. The last term describes the Coulomb interaction in the f-shell. The actual choice of these parameters will be discussed later.

This model assumes the weakness of the hybridization between the localized f-electrons and the itinerant s-, p-, and d-states described in DFT. Thus, the quantum impurity Anderson model [19] is reduced to the atomic limit, and corresponds to the Hubbard-I approximation (HIA).

The Lanczos method [21] is employed to find the lowest-lying eigenstates of the many-body Hamiltonian $H_{\rm imp}$ and to calculate the self-energy matrix $[\Sigma(z)]_{\gamma,\gamma'}$ in the subspace of the f spin-orbitals $\{\phi_\gamma = \phi_{m\sigma}\}$ at low temperature ($k_{\rm B}T = \beta^{-1} = 2$ meV). Once the self-energy is found, the local Green's function $G(z)$ for the electrons in the $4f$ manifold reads

$$G(z) = ([G(z)_{\rm DFT}]^{-1} + \Delta\epsilon - \Sigma(z))^{-1}, \quad (4)$$

where $G_{\rm DFT}(z)$ is the "noninteracting" DFT Green's function, and $\Delta\epsilon$ is chosen so as to ensure that $n_f = -\pi^{-1}{\rm Im\ Tr}\int_{-\infty}^{E_{\rm F}} dz[G(z)]$ is equal to the number of $4f$ electrons derived from Eq. (2). Then, with the aid of the local Green's function $G(z)$, we evaluate the occupation matrix $n_{\gamma_1\gamma_2} = -\pi^{-1}\,{\rm Im}\int_{-\infty}^{E_{\rm F}} dz\,[G(z)]_{\gamma_1\gamma_2}$.

This matrix $n_{\gamma_1\gamma_2}$ is used to construct an effective DFT+U potential V_U in Eq. (2). Note that the DFT potential $V_{\rm DFT}$ in Eq. (2) acting on the f-states is corrected to exclude the nonspherical double-counting with V_U [12]. Equations (2) are iteratively solved until self-consistency over the charge density is reached. The new DFT Green's function $G_{\rm DFT}$ and the new value of the $5f$-shell occupation are obtained from the solutions of Eq. (2). The next iteration is started by solving Eq. (3) with the updated value of $\epsilon_f = -\mu$ in Eq. (3), which is determined by the condition $\mu = V_{\rm dc}$ [18].

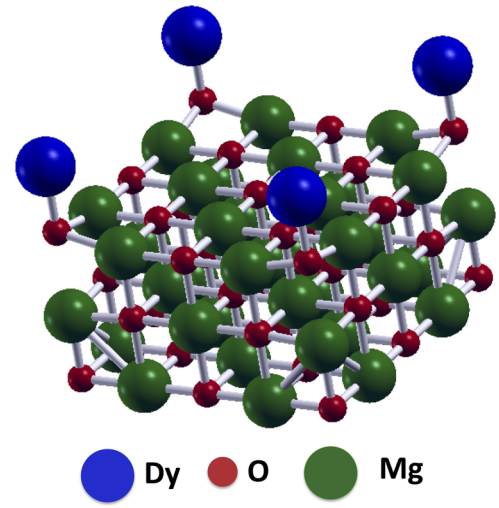

FIG. 1. Supercell model for rare-earth impurity on MgO(001). Dy atoms are shown in blue, O atoms are in red, and Mg atoms in green.

The loop procedure is repeated until the convergence of the $4f$-manifold occupation n_f is better than 0.02. After the self-consistent solution of DFT+U(HIA) is obtained, the mean-field total energy $E_{\rm tot} = E_{\rm DFT} + \Delta E^{\rm ee}$ is calculated as a sum of DFT total energy $E_{\rm DFT}$, and the energy correction $\Delta E^{\rm ee} = E^{\rm ee} - E_{\rm dc}$. Importantly, this solution is unique as it stems from the many-body ground state of Eq. (3) with the exact atomic limit.

We make use of the $2\times2\times1$ lateral supercell ($a = 4.21$ Å) of 3 ML of MgO to which the rare-earth Dy adatom is added on the oxygen site (see the supplemental material [22]). To obtain the supercell geometry, we performed the standard DFT (with the exchange-correlation functional of Perdew, Burke, and Ernzerhof [26]) Vienna ab initio simulation package (VASP [27]) calculations together with the projector augmented-wave method (PAW [28]). Moreover, assuming that localized $4f$ electrons have a rather small impact on the geometry, we used the rare-earth Lu adatom instead of Dy, and we treated 14 closed $4f$-shell electrons of Lu as valence. The system was relaxed until the forces on the Lu adatom and on the topmost 2 ML of MgO were 0.001 eV/Å. The calculated 2.1 Å Lu-O bond length to the underneath oxygen is in good quantitative agreement with the DFT+U results of Ref. [6] for the Dy-O bond length. Calculated adsorption geometry is shown in Fig. 1.

The structural information obtained from the VASP simulations was used as an input for further DFT+U(HIA) electronic structure calculations that employ the relativistic version of the full-potential linearized augmented plane-wave method (FP-LAPW) [29]. In the FP-LAPW, the SOC is included in a self-consistent second-variational procedure [30]. This two-step approach synergetically combines the speed and efficiency of the highly optimized VASP package with the state-of-the-art accuracy of the FP-LAPW method

The Slater integrals $F_0 = 7.00$ eV, and $F_2 = 9.77$ eV, $F_4 = 6.53$ eV, and $F_6 = 4.83$ eV, were chosen to parametrize the Coulomb interaction term in Eq. (3), and to construct the DFT+U potential V_U in Eq. (2). They correspond to the values for Coulomb $U = 7.00$ eV and exchange $J = 0.82$ eV. The above choice of the Slater integrals is justified [31] by agreement between the density of states (DOS) calculated with DFT+U(HIA) and the experimental valence-band photoemission for the bulk Dy.

The exchange splitting $\Delta_{\rm EX}$ in Eq. (3) corresponds to the interorbital exchange energy between the localized $4f$ and itinerant s and d shells [32,33]. The $\Delta_{\rm EX}$ can be estimated as

$$\Delta_{\rm EX} = 2J_{fs}S_{6s} + 2J_{fd}S_{5d},$$

where J_{fs} and J_{fd} are the interorbital exchange constants [33]. The spin-polarized DFT calculations with the magnetization directed along the z-axis yield $\Delta_{\rm EX} \approx 10$ meV, which can be taken as a lower bound value for the interorbital exchange energy [32].

We performed the DFT+U(HIA) calculations treating $\Delta_{\rm EX}$ as a parameter in Eq. (3). In these spin-polarized calculations, we applied the DFT non-spin-polarized exchange-correlation potential to the f-states in Eq. (2) in order to exclude the contribution of the f-intraorbital exchange field into the double-counting $V_{\rm dc}$. The spin-polarized functional is used for all other states.

We solve self-consistently Eq. (2), and we obtain the dependence of the total spin magnetic moment per unit cell $M(\Delta_{\rm EX})$ [see Fig. 2(a)] and the total energy $E^{\rm tot}(\Delta_{\rm EX})$ Eq. (1) [see Fig. 2(b)] on the magnitude of $\Delta_{\rm EX}$. Note that the upper bound limit of $\Delta_{\rm EX} \approx 40$ meV is set by reaching the saturation of the magnetic moment.

The total energy versus the magnetic moment dependence $E^{\rm tot}(M)$ is shown in Fig. 2(c). Using the Landau expansion [34] of the magnetic energy,

$$E^{\rm tot}(M) = {\rm const} + \alpha M^2 - \beta M^4,$$

we obtain the magnetic moment $M = \sqrt{\frac{\alpha}{2\beta}}$, which corresponds to the minimum of $E^{\rm tot}$. The corresponding value of $\Delta_{\rm EX} \approx 20$ meV yields the value of the interorbital exchange splitting in Eq. (3).

The inelastic electron tunneling spectroscopy (IETS) measures the magnetic excitations on an individual atom. The IETS spectra and corresponding intra-atomic exchange energy $E_{\rm EX} = 2\Delta_{\rm EX}S_{4f}$ of a Dy adatom on graphene/Cu (97 meV) and graphene/Ir(111) (90 meV) were measured experimentally [33]. For the Dy@MgO case, $E_{\rm EX} \approx 80$ meV is obtained by making use of the calculated value for $\Delta_{\rm EX} \approx 20$ meV, and $S_{4f} = 2$ according to Hund's first rule, in reasonable agreement with the available experimental data [33]. The calculated ground-state f-electron occupation $n_f = {\rm Tr}[\hat{n}]$, magnetic spin $\langle M_S\rangle = -2\langle S_z\rangle\mu_B/\hbar = -{\rm Tr}[\hat{\sigma}_z\hat{n}]\mu_B/\hbar$, orbital $\langle M_L\rangle = -\langle L_z\rangle\mu_B/\hbar$, dipole $\langle M_D\rangle = -6\langle T_z\rangle\mu_B/\hbar$ moments, and $R_{LS} = \frac{\langle M_L\rangle}{\langle M_S\rangle+\langle M_D\rangle}$ value, the ratio of the orbital to the effective spin moment, are shown in Table I. The itinerant part of the magnetization of 0.10 μ_B includes the Dy adatom $6s$-states $m_{6s} = 0.02\mu_B$, and $5d$-states $m_{5d} = 0.02\,\mu_B$ magnetic moments. Note that the calculation of these moments is associated with some uncertainty, and it depends on the choice of the Dy adatom "muffin-tin" radius.

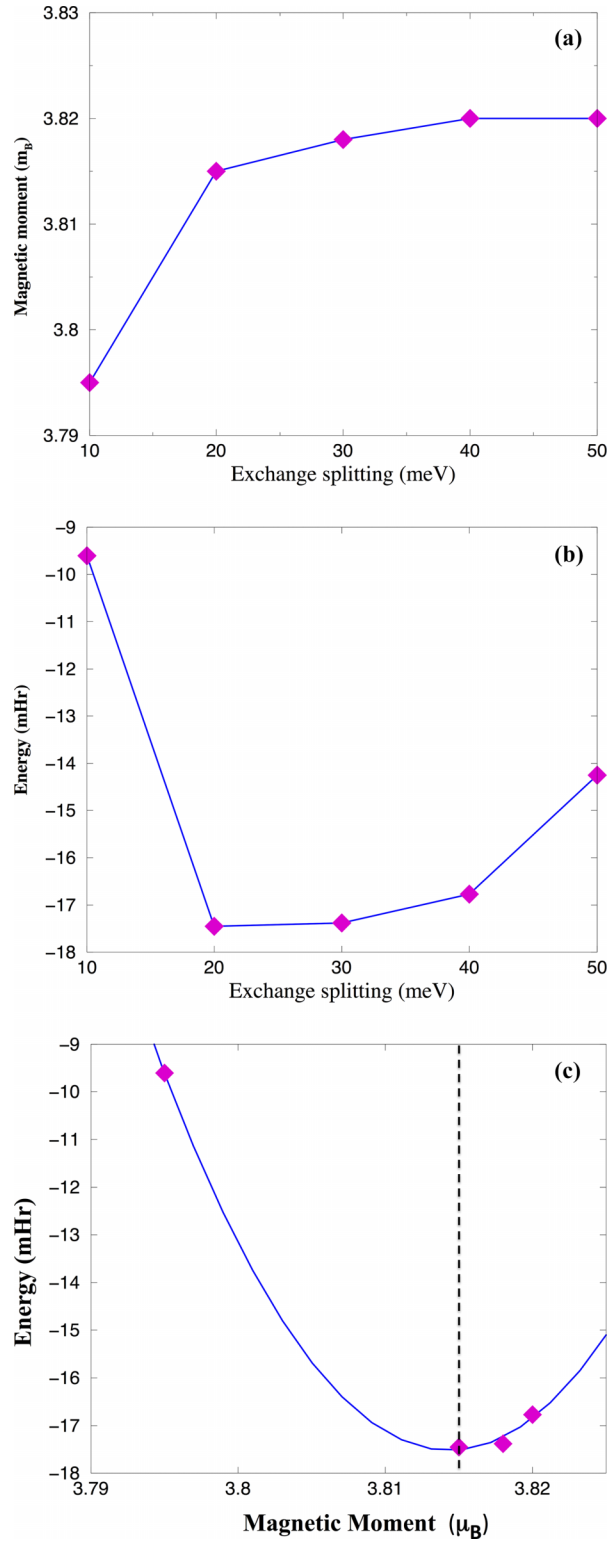

FIG. 2. The total spin magnetic moment per unit cell vs the exchange splitting $\Delta_{\rm EX}$ dependence (a); The total energy per unit cell vs the exchange splitting $\Delta_{\rm EX}$ dependence (b); the total energy as a function the magnetic moment dependence, $E^{\rm tot}(M) = {\rm const} + \alpha M^2 - \beta M^4$ (c). The total energy minimum position is marked by a dashed line.

TABLE I. The f-electron occupation n_f, spin $\langle M_S\rangle$, orbital $\langle M_L\rangle$, $\langle M_S\rangle$ plus magnetic dipole $\langle M_D\rangle$ moments (in μ_B), and the ratio $R_{LS} = \frac{\langle M_L\rangle}{\langle M_S\rangle+\langle M_D\rangle}$ for the Dy adatom on MgO(001). The nonzero Stevens parameters B_k^q (in μeV).

	n_f	$\langle M_S\rangle$	$\langle M_L\rangle$	$\langle M_S\rangle+\langle M_D\rangle$	R_{LS}
Dy@MgO	9.91	3.65	5.92	4.64	1.28
CF	B_2^0	B_4^0	B_6^0	B_4^4	B_6^4
	−20.55	0.23	−0.02	1.81	0.04

The total (TDOS) and f-projected (fDOS) DOS calculated from the solutions of Eq. (2) are shown in Fig. 3(a). The MgO band gap is at ≈ 3-to-1 eV below the Fermi level. The sharp $4f$-spin-↓ peaks are located at the top of the MgO valence band gap. The smooth TDOS peak ≈ 1 eV below the Fermi level has a capacity of two electrons, which are transferred from the Dy adatom to the MgO substrate. Note that qualitatively similar metallization of an insulating $SrTiO_3$ surface due to a Dy adatom has been reported recently [35].

The many-body ground-state solution of Eq. (3) has $N_f = 10$ (number of particles) and $J = 8$ (total moment) quantum numbers. They correspond to the f^{10} ion configuration,

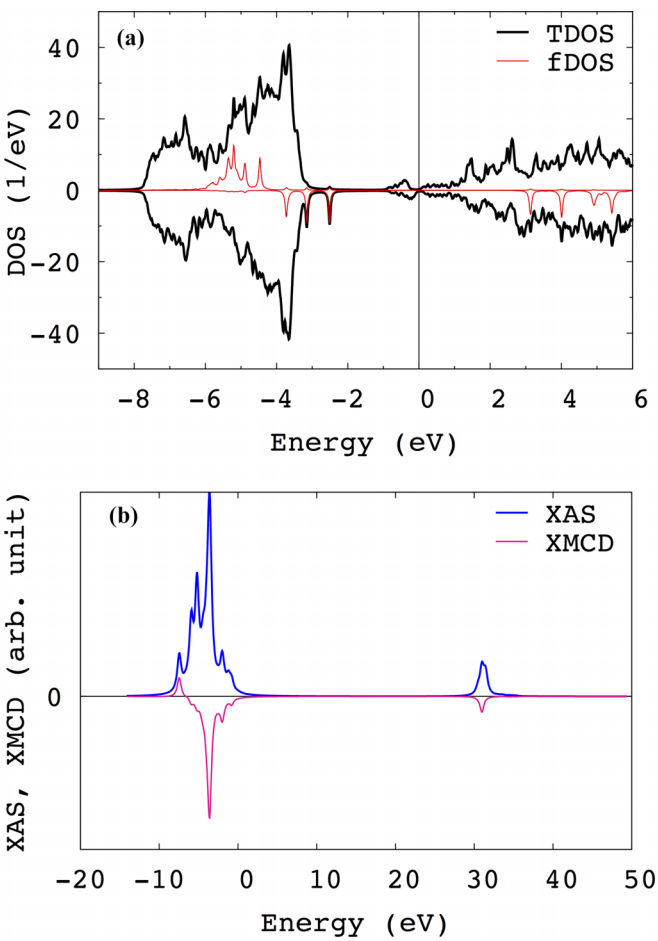

FIG. 3. The spin-resolved total (TDOS) and the f-projected (fDOS) DOS (a); the $M_{4,5}$ edge XAS and XMCD spectra (normal incidence) (b) for Dy@MgO(001).

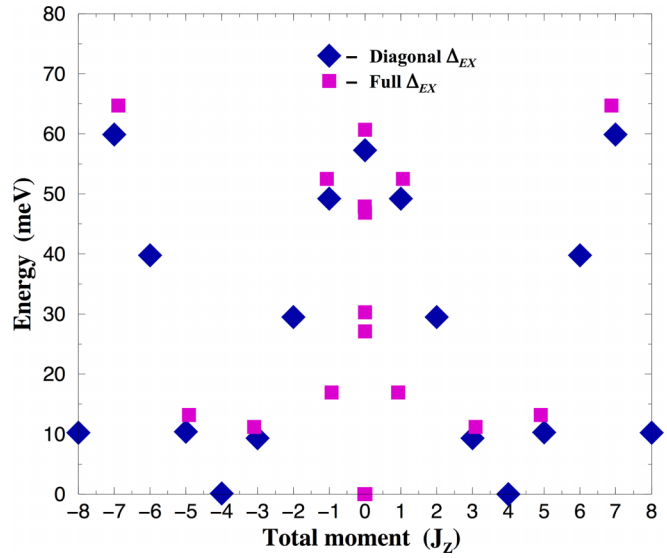

FIG. 4. Scheme of quantum many-body levels of the lowest $J = 8.0$ multiplet obtained from the solutions of Eq. (3) ($\Delta_{ex} = 0$) with the Δ_{CF} parameters taken from spin-polarized calculations (squares), with the uniaxial (diagonal) contributions to the Δ_{CF} only (diamonds).

and define the Dy adatom valence as Dy^{2+}. The f-electron occupation $n_f = 9.91$ calculated with the aid of Eq. (4) is consistent with the f^{10} configuration obtained from Eq. (3). We used Eq. (3), with the self-consistently determined parameters as an input for the Quanty code [36,37], to estimate the $M_{4,5}$-edge XAS and XMCD spectra (for details, see the supplemental material [22]). The computed spectra [Fig. 3(b)] are in reasonable agreement with available experimental data [6].

The scheme of quantum many-body levels of the lowest $J = 8.0$ multiplet obtained from the solutions of Eq. (3) is shown in Fig. 4. Without an external magnetic field, the lowest energy state of Eq. (3) is a singlet $|J = 8.0, J_z = 0.0\rangle$ state. There is another $|J = 8.0, J_z = 0.0\rangle$ singlet with the energy of 0.06 meV above the ground state. Leaving the only uniaxial (diagonal) contributions to the Δ_{CF} yields the $|J = 8.0, J_z = \pm 4.0\rangle$ ground state (cf. Fig. 4).

The Δ_{CF} matrix calculated in the DFT+U(HIA) is used to build the CF Hamiltonian [38] for the Dy@MgO(001),

$$\hat{H}_{CF} = \sum_{kq} B_k^q \hat{O}_k^q, \tag{5}$$

where $\hat{O}_k^q$ are the Stevens operator equivalents, and B_k^q are the Stevens crystal-field parameters (in standard notations) for given k and q. The five evaluated nonzero Stevens parameters—B_2^0, B_4^0, B_6^0, B_4^4, and B_6^4—are shown in Table I. The energy diagrams of the CF Hamiltonian (5) are shown in Fig. S2 (see the supplemental material [22]). Both diagrams, with the full set of the CF parameters, and with the first three uniaxial CF parameters, are shown. It is seen that the CF solutions approximate reasonably well the many-body solutions of Eq. (3) shown in Fig. 4.

The first three parameters B_2^0, B_4^0, B_6^0 yield the uniaxial splitting between different J_z eigenstates in Eq. (5) with the $|J = 8.0, J_z = \pm 4.0\rangle$ ground state, and they correspond to diagonal contributions to the Δ_{CF}. The energy difference

between the lowest and highest J_z levels, the so-called zero-field splitting (ZFS) of 65 meV, is found, which is related to the uniaxial magnetic anisotropy [39]. The transverse $B_4^4O_4^4$ term in the CF Hamiltonian connects the $|J = 8.0, J_z = \pm 4.0\rangle$ states so that the quantum tunneling of the magnetization (QTM) occurs between these two states, and the resulting $|J = 8.0, J_z = 0\rangle$ ground state corresponds to the "in-plane" magnetic moment orientation. It explains an absence of the remanent magnetization in Dy@MgO(001) observed experimentally [6].

The giant magnetic anisotropy energy of 250 meV for a Dy adatom on top of a [2 ML-MgO]/Ag(001) film has been recently observed [3]. As follows from the analysis of the experimental data [6], a Dy adatom has a $4f^9$, $J = 7.5$ ground state, which is protected from QTM. This MAE exceeds substantially our estimated value of 65 meV for the uniaxial MAE for Dy@[3ML-MgO]. A drastic effect of an Ag substrate has been recently reported for a Fe-phthalocyanine (Pc) molecule absorbed on MgO, where it was shown that the spin of the molecule shifts from $S = 1$ to $S = \frac{1}{2}$ due to the presence of an Ag substrate [40]. We anticipate that an Ag substrate will play a very essential role in the formation of a $4f^9$, $J = 7.5$ ground state for a Dy adatom on ultrathin MgO/Ag films, and we will give it further consideration.

To conclude, the electronic structure and magnetism of an individual Dy atom adsorbed on the MgO(001) substrate is investigated using a combination of the density functional theory with the Hubbard-I approximation to the Anderson impurity model. The divalent Dy^{2+} adatom is found with a singlet $|J = 8.0, J_z = 0.0\rangle$ ground state. The calculated XAS and XMCD spectra are in reasonable agreement with available experimental data. No remanent magnetization is found due to QTM, in agreement with an experimentally observed butterfly-type magnetic hysteresis loop.

We acknowledge stimulating discussions with J. Kolorenc and A. Yu. Denisov. Financial support was provided by Operational Programme Research, Development and Education financed by European Structural and Investment Funds and the Czech Ministry of Education, Youth and Sports (Project No. SOLID21-CZ.02.1.01/0.0/0.0/16_019/0000760), by the Czech Science Foundation (GACR) Grant No. 22-22322S, and from the Israeli Ministry of Aliyah and Integration (MOIA) Grant No. 714471.

[1] F. Donati and A. J. Heirich, A perspective on surface-adsorbed single atom magnets as atomic-scale magnetic memory, Appl. Phys. Lett. **119**, 160503 (2021).

[2] S. Thiele, F. Balestro, R. Ballou, S. Klyatskaya, M. Ruben, and W. Wernsdorfer, Electrically driven nuclear spin resonance in single-molecule magnets, Science **344**, 1135 (2014).

[3] A. Singha, P. Willke, T. Bilgeri, X. Zhang, H. Brune, F. Donati, A. J. Heinrich, and T. Choi, Engineering atomic-scale magnetic fields by dysprosium single atom magnets, Nat. Commun. **12**, 4179 (2021).

[4] C. A. P. Goodwin, F. Ortu, D. Reta, N. F. Chilton, and D. P. Mills, Nature (London) **548**, 439 (2017).

[5] R. Baltic, M. Pivetta, F. Donati, C. Wackerlint, A. Singha, J. Dreiser, S. Rusponi, and H. Brune, Superlattice of Single Atom Magnets on Graphene, Nano Lett. **16**, 7610 (2016).

[6] F. Donati, M. Pivetta, C. Wolf, A. Singha, C. Wackerlin, R. B. de Groot, S. L. Ahmed, L. Persichetti, C. Nistor *et al.*, Correlation between Electronic Configuration and Magnetic Stability in Dysprosium Single Atom Magnets, Nano Lett. **21**, 8266 (2021).

[7] A. Uldry, F. Vernay, and B. Delley, Systematic computation of crystal-field multiplets for x-ray core spectroscopies, Phys. Rev. B **85**, 125133 (2012).

[8] A. B. Shick, A. I. Liechtenstein, and W. E. Pickett, Implementation of the LDA+U method using the full-potential linearized augmented plane-wave basis, Phys. Rev. B **60**, 10763 (1999).

[9] A. B. Shick and W. E. Pickett, Magnetism, spin-orbit coupling, and superconducting pairing in UGe_2, Phys. Rev. Lett. **86**, 300 (2001).

[10] V. I. Anisimov, J. Zaanen, and O. K. Andersen, Band theory and Mott insulators: Hubbard U instead of Stoner I, Phys. Rev. B **44**, 943 (1991).

[11] I. V. Solovyev, P. H. Dederichs, and V. I. Anisimov, Corrected atomic limit in the local-density approximation and the electronic structure of d impurities in Rb, Phys. Rev. B **50**, 16861 (1994).

[12] O. Kristanovski, A. B. Shick, F. Lechtermann, and A. I. Lichtenstein, Role of nonspherical double counting in DFT+DMFT: Total energy and structural optimization of pnictide superconductors, Phys. Rev. B **97**, 201116(R) (2018).

[13] A. B. Shick, W. E. Pickett, and A. I. Liechtenstein, Ground and metastable states in γ-Ce from correlated band theory, J. Electron. Spectrosc. Relat. Phenom. **114-116**, 753 (2001).

[14] B. Dorado, M. Freyss, B. Amadon, M. Bertolus, G. Jomard, and P. Garcia, Advances in first-principles modelling of point defects in UO_2: f electron correlations and the issue of local energy minima, J. Phys.: Condens. Matter **25**, 333201 (2013).

[15] M. Krack, On the ground state electronic structure of uranium dioxide, Phys. Scr. **90**, 094014 (2015).

[16] B. Dorado, G. Jomard, M. Freyss, and M. Bertolus, Stability of oxygen point defects in UO_2 by first-principles DFT+U calculations: Occupation matrix control and Jahn-Teller distortion, Phys. Rev. B **82**, 035114 (2010).

[17] B. Meredig, A. Thompson, H. A. Hansen, C. Wolverton, and A. van de Walle, Method for locating low-energy solutions within DFT+U, Phys. Rev. B **82**, 195128 (2010).

[18] A. B. Shick, S.-I. Fujimori, and W. E. Pickett, UTe_2: a nearly insulating half-filled j=5/2, $5f^3$ heavy fermion metal, Phys. Rev. B **103**, 125136 (2021).

[19] A. Hewson, *The Kondo Problem to Heavy Fermions* (Cambridge University Press, Cambridge, 1993).

[20] A. H. MacDonald, W. E. Pickett, and D. L. Koelling, A linearised relativistic augmented-plane-wave method utilising approximate pure spin basis functions, J. Phys. C **13**, 2675 (1980).

[21] J. Kolorenč, A. I. Poteryaev, and A. I. Lichtenstein, Valence-band satellite in ferromagnetic nickel: LDA+DMFT study with exact diagonalization, Phys. Rev. B **85**, 235136 (2012).

[22] See Supplemental Material at http://link.aps.org/supplemental/10.1103/PhysRevB.108.L180408. for the details of the electronic structure calculations, a comparison with the experimental XAS and XMCD spectra, and the energy diagram of the CF Hamiltonian. The supplemental material also contains Refs. [23–25].

[23] A. Singha, R. Baltic, F. Donati, Ch. Wackerlin, J. Dreiser, L. Persichetti, S. Stepanow, P. Gambardella, S. Rusponi, and H. Brune, $4f$ occupancy and magnetism of rare-earth atoms adsorbed on metal substrates, Phys. Rev. B **96**, 224418 (2017).

[24] R. D. Cowan, *The Theory of Atomic Structure and Spectra* (University of California Press, Berkeley, 1981).

[25] J. A. Bearden and A. F. Burr, Reevaluation of X-Ray Atomic Energy Levels, Rev. Mod. Phys. **39**, 125 (1967).

[26] J. P. Perdew, K. Burke, and M. Ernzerhof, Generalized Gradient Approximation Made Simple, Phys. Rev. Lett. **77**, 3865 (1996).

[27] G. Kresse and J. Furthmuller, Efficient iterative schemes for ab initio total-energy calculations using a plane-wave basis set, Phys. Rev. B **54**, 11169 (1996).

[28] P. E. Blöchl, Projector augmented-wave method, Phys. Rev. B **50**, 17953 (1994).

[29] E. Wimmer, H. Krakauer, M. Weinert, and A. J. Freeman, Full-potential self-consistent linearized-augmented-plane-wave method for calculating the electronic structure of molecules and surfaces: O_2 molecule, Phys. Rev. B **24**, 864 (1981).

[30] A. B. Shick, D. L. Novikov, and A. J. Freeman, Relativistic spin-polarized theory of magnetoelastic coupling and magnetic anisotropy strain dependence: Application to Co/Cu(001), Phys. Rev. B **56**, R14259(R) (1997)

[31] A. B. Shick, J. Kolorenc, A. Y. Denisov, and D. S. Shapiro, Magnetic anisotropy of a Dy atom on a graphene/Cu(111) surface, Phys. Rev. B **102**, 064402 (2020).

[32] L. Peters, I. Di Marco, P. Thunström, M. I. Katsnelson, A. Kirilyuk, and O. Eriksson, Treatment of 4f states of the rare earths: The case study of TbN, Phys. Rev. B **89**, 205109 (2014).

[33] M. Pivetta, F. Patthey, I. Di Marco, A. Subramonian, O. Eriksson, S. Rusponi, and H. Brune, Measuring the Intra-Atomic Exchange Energy in Rare-Earth Adatoms, Phys. Rev. X **10**, 031054 (2020).

[34] L. D. Landau, and E. M. Lifshits, *Statistical Physics*, 3rd ed. (Elsevier, Amsterdam, 1980), Pt. 1.

[35] V. Bellini, S. Rusponi, J. Kolorenc, S. K. Mahatha, M. A. Valbuena, L. Persichetti, M. Pivetta, B. V. Sorokin, D. Merk, S. Reynaud, D. Sblendorio *et al.*, ACS Nano **16**, 11182 (2022).

[36] M. W. Haverkort, M. Zwierzcki, and O. K. Andersen, Multiplet ligand-field theory using Wannier orbitals, Phys. Rev. B **85**, 165113 (2012).

[37] https://quanty.org.

[38] A. B. Shick and A. Yu. Denisov, Magnetism of $4f$-atoms adsorbed on metal and graphene substrates, J. Magn. Magn. Mater. **475**, 211 (2019).

[39] R. Baltic, F. Donati, A. Singha, R. Baltic, Ch. Wackerlin, J. Dreiser, B. Delley, M. Pivetta, S. Rusponi, and H. Brune, Magnetic properties of single rare-earth atoms on graphene/Ir(111), Phys. Rev. B **98**, 024412 (2018).

[40] X. Zhang, C. Wolf, Y. Wang, H. Aubin, T. Bilgeri, P. Willke, A. J. Heinrich, and T. Choi, Electron spin resonance of single iron phthalocyanine molecules and role of their non-localized spins in magnetic interactions, Nat. Chem. **14**, 59 (2022).